Sixth International Symposium on Turbulence and Shear Flow Phenomena
Seoul, Korea, 22-24 June 2009

LARGE EDDY SIMULATION OF A TURBULENT JET FLAME

Saugata Chakravorty, Joseph Mathew
Department of Aerospace Engineering,
Indian Institute of Science,
Bangalore 560012 INDIA
saugatac@aero.iisc.ernet.in, joseph@aero.iisc.ernet.in

ABSTRACT

A Large eddy simulation of a turbulent reacting round jet (Sandia Flame D) was performed. The sub-grid stress arising out of non-linearities of the governing equations were modeled using the explicit filtering approach. A posteriori comparisons with benchmark experiments indicate that the explicit filtering method suffices to model the effect of sub-grid stress on the filtered velocity field for non-reacting flow. However, in the presence of reaction the sub-grid scale effects arising from the strong non-linearity of the reaction rate is poorly accounted for, leading to a discrepancy between experiment and simulation.

INTRODUCTION

Among the remaining challenges for large eddy simulation (LES) is the need to understand how to simulate flows in which phenomena at scales smaller than the discretization play an important role. A most important application of this type is turbulent combustion. In many cases the flames are very thin—much thinner than the grid spacing that is adequate for LES of non-reacting flow at the same Reynolds numbers. So the effect of the flame on the evolution of the computed large scale part must be modelled. Suppose the flame thickness to be $O(\lambda_f)$ and grid spacing Δ. When $\lambda_f \ll \Delta$, the use of flamelet models have been successful (see, Pitsch (2005) for a recent review of the various approaches). When $\lambda_f \sim \Delta$, it is possible to artificially thicken the flame so that flame structure can be represented on a feasible grid. Our present investigations are to determine whether the more general pdf-type approach proposed in Colucci *et al.* (1998) & Jaberi *et al.* (1999), combined with the filtering approach to LES (Mathew *et al.*, 2003) is useful. The generality lies in that, in principle, the approach is not restricted to thin flames. So it is especially useful when the reaction zones of different species vary widely and the expectations of a flamelet models are not met. The flame chosen for simulation studies is the partially-premixed, piloted, round-jet, methane flame at moderate jet speeds known as the SANDIA flame D from benchmark experiments (Barlow & Frank, 2003) of a series of flames.

FORMULATION

Governing Equations

The governing equations for the compressible flow of a perfect gas undergoing chemical reaction with heat release are the equations for conservation of mass, momentum and energy, transport equations for reactant mass fractions and the equation of state (Williams, 1985). For low Mach number ($\mathrm{M} \ll 1$) flows, direct integration of these compressible equations are computationally expensive because of the severe restriction on the time step due to acoustic wave propagation. This restriction can be circumvented by performing a low Mach number expansion of the governing equation. When the essential dynamics in flows such as low-speed combustion is dependent on density differences but not on compressibility, this procedure improves computational efficiency. Following Majda & Sethian (1985) the low Mach number equations are,

$$\frac{\partial \rho}{\partial t} + \nabla \cdot (\rho \mathbf{U}) = 0, \tag{1}$$

$$\rho \frac{\partial \mathbf{U}}{\partial t} + \rho \mathbf{U} \cdot \nabla \mathbf{U} = -\nabla p^{(1)} + \frac{1}{\mathrm{Re}} \nabla \cdot \tau, \tag{2}$$

$$\nabla \cdot \mathbf{U} = \frac{1}{\gamma p^{(0)}} \left[\frac{\gamma}{\mathrm{PrRe}} \nabla^2 T - \frac{\mathrm{d}p^{(0)}}{\mathrm{d}t} + H(R_i) \right], \tag{3}$$

$$\rho \frac{\partial Z}{\partial t} + \rho \mathbf{U} \cdot \nabla Z = \frac{1}{\mathrm{ScRe}} \nabla^2 Z \tag{4}$$

$$\rho \frac{\partial C}{\partial t} + \rho \mathbf{U} \cdot \nabla C = \frac{1}{\mathrm{ScRe}} \nabla^2 C + R_i \tag{5}$$

$$p^{(0)} = \rho T \tag{6}$$

Here, velocity $\mathbf{U}$, density ρ, temperature T, and lengths $\mathbf{x}$ were scaled with their respective reference quantities $U_\infty, \rho_\infty, T_\infty$ and L_∞. The pressure $p^{(0)}$ represents the thermodynamic pressure and does not take part in the fluid dynamic process. Pressure $p^{(1)}$ is the hydrodynamic pressure. Pressure was non-dimensionalized with the reference thermodynamic pressure $\rho_\infty \mathcal{R} T_\infty$, where $\mathcal{R}$ is the universal gas constant, and time t by L_∞ / U_∞. $H = H(R_i)$ is the heat source term. $R_i = R(\rho, C_i, T)$ is the reaction rate. Chemistry was modeled as a single single step, irreversible reaction of the form,

$$\mathrm{CH_4} + 2\ \mathrm{O_2} \rightarrow \mathrm{CO_2} + 2\mathrm{H_2O} + \text{heat}.$$

Transport coefficients and specific heats were taken as functions of temperature. Three non-dimensional parameters appearing in equations (2)–(5), are the Reynolds number $Re = \rho_\infty U_\infty L_\infty / \mu_\infty$, the Prandtl number $Pr = c_{p_\infty} \mu_\infty / k_\infty$ and the Schmidt number $Sc = \mu_\infty / \rho_\infty D_\infty$. The heat release ($H(R_i)$) and the reaction source term (R_i) appearing in equation (3) and (5) were modeled using an Arrhenius type rate equation. Then the rate of consumption or generation of fuel ($F \equiv CH_4$), oxidizer ($O \equiv O_2$) and product ($P \equiv CO_2$ & H_2O) are

$$R_F = R_O = -R_P = \mathrm{Da}\ \rho C_F \rho C_O \exp(-Ze/T), \tag{7}$$

and the heat release term,

$$H = \text{Ce Da } \rho C_F \rho C_O \exp(-Ze/T)/C_p. \quad (8)$$

The non-dimensional parameters appearing in the reaction rate are the Damkohler number, $Da = \rho K_\infty L_\infty / U_\infty$, where K_∞ is the reaction rate parameter and Zeldovich number $Ze = E_a/RT_\infty$, where E_a is the activation energy. The non-dimensional heat release factor $\text{Ce} = C_\infty \triangle H/\rho_\infty C_{p\infty} T_\infty$, where $C_{p\infty}$ is the reference specific heat at constant pressure and $\triangle H$ is the heat of reaction. Solutions were obtained by integrating equations (2), (4) and (5) subject to the constraints imposed by equations (1), (3), (6).

Numerical Method

The governing equations were discretized in cylindrical coordinate using a partially staggered grid (Lowery & Reynolds, 1986). Spectral-like fourth-order compact difference schemes (Lele, 1992; Chakravorty & Mathew, 2004), were used to evaluate the spatial derivatives. The improved resolution offered by the compact differencing scheme leads to increased possibility of aliasing error. In the present simulation no explicit de-aliasing algorithm has been used, but the skew-symmetric form of discretization employed here does provide for high wavenumber filtering. Where needed, interpolations were done using high-resolution formulas The convective part of scalar transport equations were discretized using the 5th-order WENO scheme of Jiang & Shu (1996). The conservation equations were integrated in time using 2nd-order accurate Runge-Kutta scheme. Traction free condition was used along the lateral boundary to allow for entrainment of flow into the jet. Along the outflow plane, advective boundary condition was imposed (Akselvoll & Moin, 1995).

Large Eddy Simulation

The sub-grid scale effects of the flow field were modeled using an explicit filtering procedure (Mathew *et al.*, 2003). The method follows from the approximate deconvolution model of Stolz & Adams (1999). The deconvolution approach is a mathematically consistent way of approximating the unresolved scale based on the solution of the filtered governing equations. The method consists of a primary filtering operation followed by a deconvolution step to approximate the unclosed terms arising out of filtering the governing equations. It has been shown in Mathew *et al.* (2003) that this two steps of primary filtering and approximate deconvolution when implemented sequentially on a code reduces to a single explicit filtering step. In the present study optimized fourth-order implicit filters of Lele (1992) were used. These filters have the property that they are perfect low-pass filters. The low wavenumber modes of the solution are left unchanged in the filtering operation and at the same time the filter falls smoothly to zero beyond a certain filter cut-off value. Figure 1 shows the transfer function for the various interpolation , differentiation and the filter operators used in the present study.

FMDF method

Jaberi *et al.* (1999) developed a method called the Filtered Mass Density Function (FMDF) to model the effects of the subgrid scalar fluctuations in variable density reacting flows. In this approach, the sub-grid scalar fluctuations are treated in a probabilistic manner and their evolution in time is obtained by solving a modeled transport equation.

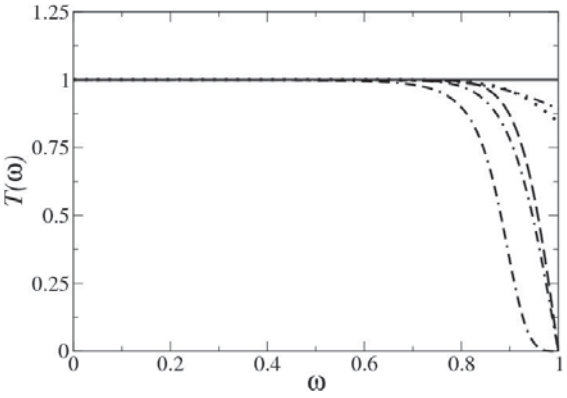

Figure 1: Transfer functions:: $--$: interpolation; $- \cdot -$: first derivative (standard); $- \cdot\cdot$: first derivative (staggered); $\cdots$: second derivative; $- - \cdot$: filter; ——: exact.

Let $\phi(\mathbf{x}, t)$ denote transported scalars ($\phi_1 = Z, \phi_2 = C$, etc). The filtered mass density function, F_L, is thus defined as,

$$F_L(\psi; \mathbf{x}, t) = \int_{-\infty}^{+\infty} \rho(\mathbf{x}', t)\zeta[\psi, \phi(\mathbf{x}', t)]G(\mathbf{x}' - \mathbf{x})\mathrm{d}\mathbf{x}', \quad (9)$$

$$\zeta[\psi, \phi(\mathbf{x}, t)] = \delta[\psi - \phi(\mathbf{x}, t)] \equiv \Pi_{\alpha=1}^{N} \delta[\psi_\alpha - \phi_\alpha(\mathbf{x}, t)] \quad (10)$$

where, ψ are the composition space scalar values and $\zeta[\psi, \phi(\mathbf{x}', t)]$ is the fine-grained density. The transport equation for $F_L(\psi; \mathbf{x}, t)$ may be written as (Jaberi *et al.*, 1999),

$$\frac{\partial F_L(\psi, \mathbf{x}', t)}{\partial t} + \frac{\partial < \overline{u(\mathbf{x}, t)|\psi} > F_L(\psi, \mathbf{x}', t)}{\partial x_i} = \frac{\partial}{\partial \psi_i}\Big[\Big\langle -\overline{\frac{1}{\widetilde{\rho}(\phi)} \frac{\partial}{\partial x_i}\Big(\frac{1}{ReSc}\frac{\partial \phi_i}{\partial x_i}\Big)|\psi}\Big\rangle F_L(\psi, \mathbf{x}', t)\Big] - \frac{\partial [R(\psi) F_L(\psi, \mathbf{x}', t)]}{\partial \psi_i}. \quad (11)$$

The above equation represents the evolution of the filtered mass density function of a transported scalar exactly. The statistical information for any scalar field is obtained by integrating in the scalar composition space. In the above equation the chemical source term (the last term) appears in closed form. The conditionally filtered terms appearing in the above equation represents the sub-grid contributions. These terms are unclosed and needs to be modeled. The conditionally filtered term on the left hand side represents the sub-grid convection and that on the right hand side represent sub-grid mixing. Elsewhere, sub-grid-scale terms arising from convection were closed using an eddy viscosity model with the resolved strain rate and a kinetic energy(Jaberi *et al.*, 1999). Here we use FMDF with the explicit filtering approach for convection terms. An Interaction by Exchange with the Mean(IEM) type mixing model has been used for sub-grid mixing (Pope, 1982).

RESULTS

Incompressible Round Jet

Large eddy simulation of an unconfined, isothermal, uniform density round jet was performed at a Reynolds number, $Re = 11,000$ based on nozzle exit diameter (D) and mean centerline velocity ($U_{CL}|x = 0$) at nozzle exit. This corresponds to the air jet experiments of Panchapakesan & Lumley (1993). The computational domain in the axial

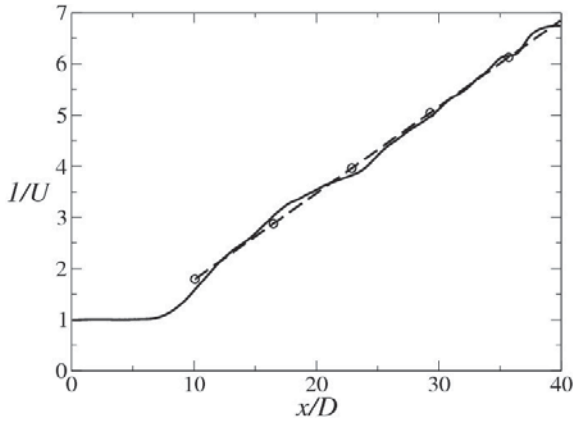

Figure 2: Variation of the reciprocal of the mean centerline axial velocity, U (normalized by jet centerline velocity at nozzle exit $U_{CL|x=0}$) with distance from the nozzle exit ($x/D = 0$). ——: simulation; $-\ \bigcirc\ -$: theoretical.

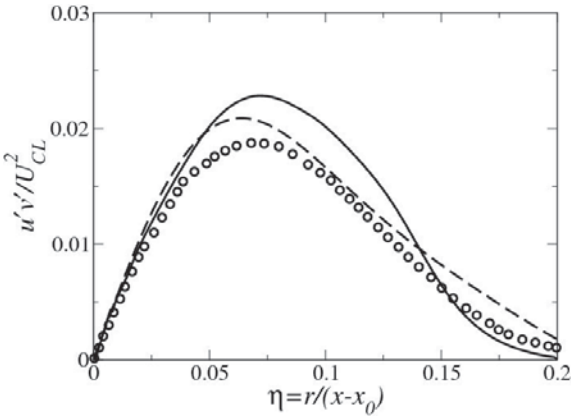

Figure 3: Turbulent shear stress profile (normalized by the local mean axial velocity U_{CL}^2) versus non-dimensional radial coordinate, η.—— : simulation; $-\ -$: Hussein *et al.* (1994); ○:Panchapakesan & Lumley (1993).

direction was $40D$ and in radial direction $10D$. The computational grid consists of $256 \times 160 \times 40$ points in the axial, radial and azimuthal direction, respectively. At nozzle exit a top hat velocity profile was assumed. Small perturbations of amplitude 1% was added to the mean flow to trigger transition to turbulence. A weak coflow of 5% of the peak inflow nozzle velocity was imposed. The simulation was initially run for 240 non-dimensional time units $D/U_{CL|x=0}$ to allow the flow to develop into a statistically stationary state after which turbulence statistics (time-averages) were collected.

Figure 2 shows the evolution of the reciprocal of the centerline axial velocity U_{CL} (——) with distance from the nozzle exit. Also shown in the same figure is the theoretical decay rate ($-\ \bigcirc\ -$)

$$\frac{U_{CL|x=0}}{U_{CL}} = \frac{1}{B_u}\left[\frac{x}{D} - \frac{x_0}{D}\right], \tag{12}$$

where x_0 is the virtual origin and B_u is the decay constant. B_u varies from 5.4 (Wygnanski & Fiedler, 1969) to 6.06 (Panchapakesan & Lumley, 1993) depending on the experimental and initial conditions. In the present study, $B_u = 5.9$ and $x_0 = -0.52$ which agrees well with the values reported previously (Wygnanski & Fiedler, 1969; Panchapakesan & Lumley, 1993; Hussein *et al.*, 1994) and (Boersma *et al.*, 1998) .

Figure 3 shows the variation of Reynolds shear stress across the jet in nondimensional radial coordinate, $\eta = r/(x - x_0)$. These profiles were obtained by averaging the nondimensional profiles over $12.5d < x/D < 32.5$. Also shown in the same figure are the measurements of Panchapakesan & Lumley (1993) and Hussein *et al.* (1994) (hot-wire). Although, the simulation does overpredict the mean Reynolds stress in the region ($0.05 < \eta < 0.15$), the overall agreement with the experimental results is quite good. This discrepancy is probably due to the difference in the problem set up. The experiments of (Panchapakesan & Lumley, 1993), (Hussein *et al.*, 1994) were performed without any coflow, whereas for computational reasons the jet in the present study was surrounded by a weak coflow.

SANDIA FLAME D

The flame chosen for simulation is the partially premixed methane/air flame of Barlow & Frank (2003) (Sandia Flame D) which is well-documented for benchmarking. At the inflow plane, the fuel jet ($25\%CH_4$: 75% dry air by volume) emerges from a circular port of diameter 7.2 mm with a mean velocity of 49.6 m/s with a parabolic profile at 294 K. A pilot flame of mean velocity 11.4 m/s and a nearly flat profile at 1880 K occupies a concentric annulus between diameters 7.7 mm and 18.2 mm. Outside the pilot is a weak co-flow of 0.9 m/s. The shear layers at jet boundaries are thin. The Reynolds number based on bulk fuel jet velocity, its viscosity and port diameter is 22400. At the inflow boundary mean experimental profiles given in Barlow & Frank (2003) were imposed for velocity, temperature, mixture fraction and CH_4 mass fraction. Random perturbations were added to the inflow mean velocity field to facilitate transition to turbulence. The random perturbations were chosen in such a way that the rms of the fluctuations matches the experimental data. In the experiments, the flame length is about 65 diameters. At this time, the jet flame has been simulated in a domain extending $20D$ in the axial direction and $5D$ in the radial direction. There were 128, 80 and 40 grid points in the axial, radial and azimuthal directions, respectively. Only the explicit filtering method has been applied. So the reaction rate term does not have any contribution from scales which

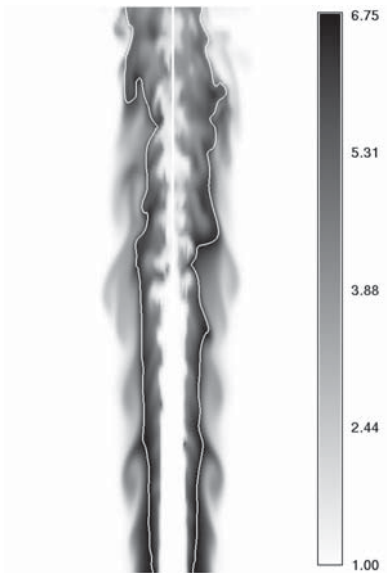

Figure 4: Stoichiometric mixture fraction (white line) superimposed on temperature isosurfaces.

are too small to be represented on the grid. This method is expected to provide a reasonable simulation where the flame is not too thin and turbulent fluctuations are not too strong.

Figure 4 shows the temperature on a longitudinal section through the flame. Also shown in the same figure the stoichiometric contour $Z = 0.355$ (white line). The stoichiometric surface closely follows the region of high temperature. Close to the nozzle exit, due to the high temperature of the pilot jet, the viscosity increases about 5 times. Owing to this increased viscosity and reduced density, the flow evolves like a laminar jet. Around $x/D = 8$ instability waves appear, roll-up and then breakdown into a turbulent state at around $12D$. Beyond $12D$ the flow is completely turbulent.

In figures 5–7 centerline evolution of mean and rms of the axial velocity, mixture fraction and temperature will be presented for the entire streamwise length of the domain. However, discussion will be limited upto $x < 16$ to discard the effects arising out of outflow boundary conditions. Figure 5 shows the centerline variation of the mean (U) and

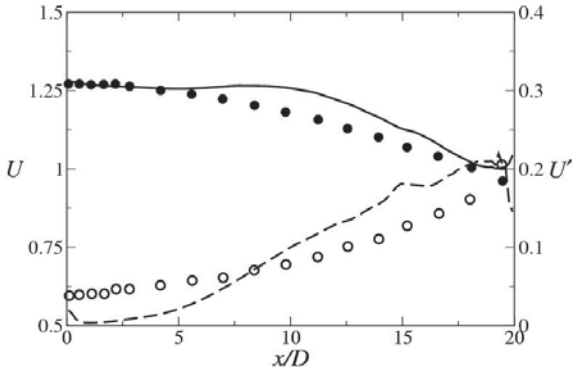

Figure 5: Centerline evolution of mean (U) and rms (U') of axial velocity component. ——: mean (simulation); – –: rms (simulation); ●: mean (experiment); ○: rms (experiment).

the rms (U') of the axial velocity component, normalized by bulk velocity at the nozzle exit. Close to the nozzle exit ($x \leq 5D$) all the velocity fluctuations have disappeared and the mean velocity evolves like a laminar flow; only beyond $x > 5D$ does the flow show the growth of velocity fluctuation. This does not necessarily imply that the explicit filtering is dissipative as in our calculation of the incompressible round jet at Re = 11000 the method was able to correctly predict the experimentally reported centerline rms of $20\% - 30\%$. A more likely cause could be the random perturbations that were introduced at the inflow plane. Such perturbations provide only the intensity and not the phase relations between different turbulent modes. This leads to the damping of the fluctuations and only after sufficient distance downstream does the flow recover and develop realistic turbulence properties (Akselvoll & Moin, 1995; Le & Moin, 1994).

Figures 6 and 7 show the centerline variation of mean and rms of mixture fraction (Z) and temperature (T), respectively, as predicted by the LES. Both the mean mixture fraction and temperature follows the experimental results closely, however differences show up in their rms values. Close to the nozzle exit none of the scalars show any fluctuations and only beyond $x/D > 10$ do they show any growth, but are nonetheless underpredicted. However, as suggested by Pitsch (2005), the underprediction of these scalars in the near field of the jet ($x < 15D$) could be due to experimental uncertainties as all the scalar rms should fall to zero at the nozzle exit.

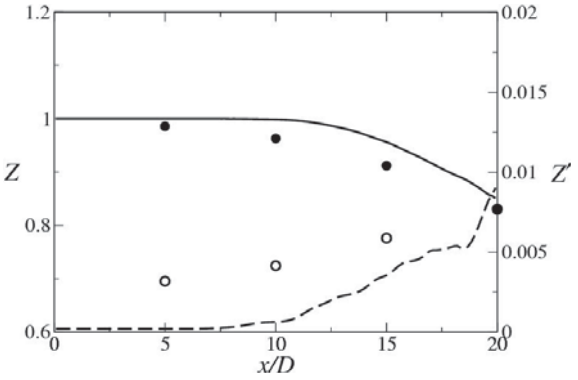

Figure 6: Centerline evolution of mean (Z) and rms (Z') mixture fraction. ——: mean (simulation); – –: rms (simulation); ●: mean (experiment); ○: rms (experiment).

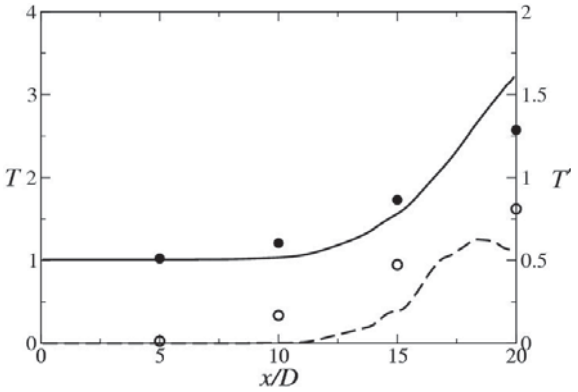

Figure 7: Centerline evolution of mean (T) and rms (T')temperature. ——: mean (simulation); – –: rms (simulation); ●: mean (experiment); ○: rms (experiment).

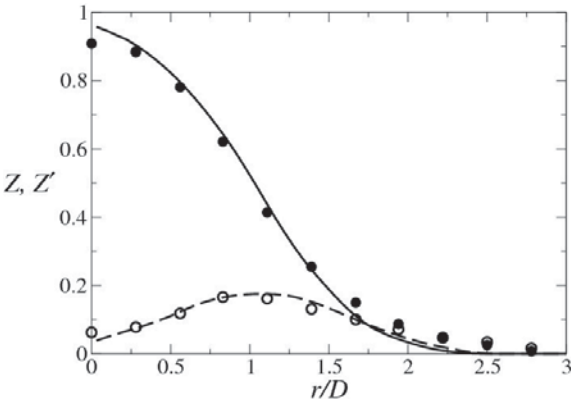

Figure 8: Radial mean and rms profile of mixture fraction at $x/D = 15$. ——: mean (simulation); – –: rms (simulation); ●: mean (experiment); ○: rms (experiment).

Figures 8, 9 and 10 show the radial profile of mean and rms of mixture fraction, temperature and CH_4, respectively, at $x/D = 15$. Mixture fraction mean and rms follows the experimental results closely but deviations appear in the temperature and CH_4 profiles. The temperature profile shows a lower peak value and less spreading in the radial direction. In fact, beyond $r/D < 1$ the temperature profile drops off rapidly while the CH_4 profile shows a sharp decrease in the fuel rich region ($r/D < 1$). A similar feature was observed in the radial profiles of mixture fraction, temperature and CH_4 at $x/D = 7.5$ (not reported here). To

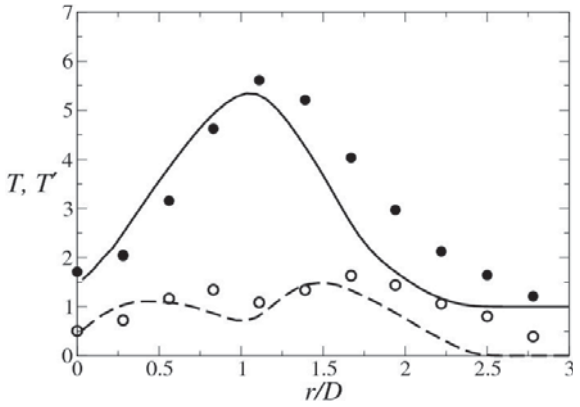

Figure 9: Radial mean and rms profile of temperature at $x/D = 15$. ——: mean (simulation); – –: rms (simulation); ●: mean (experiment); ○: rms (experiment).

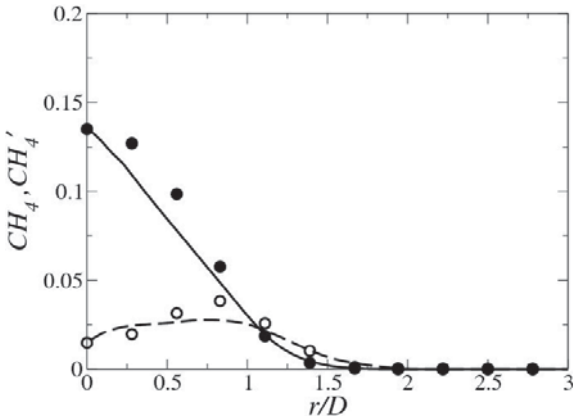

Figure 10: Radial mean and rms profile of CH_4 mass fraction at $x/D = 15$. ——: mean (simulation); – –: rms (simulation); ●: mean (experiment); ○: rms (experiment).

explain the discrepancies appearing in the radial profiles it is necessary understand the reaction zone structure at these locations in terms of the time averages of temperature and CH_4 conditioned on the mixture fraction.

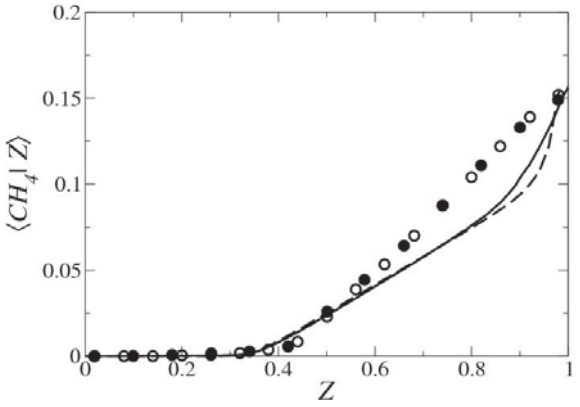

Figure 11: Conditional mean CH_4. $x/D = 7.5$::– –: simulation; ○: experiment. $x/D = 15$::——: simulation; ●: experiment.

Figures 11 and 12 shows the conditional averages at $x/D = 7.5$ & 15 for CH_4 and temperature, respectively. The conditional averages for both CH_4 and temperature follows the experimental results closely in the fuel lean region, but differs significantly in the fuel rich regions. The lower

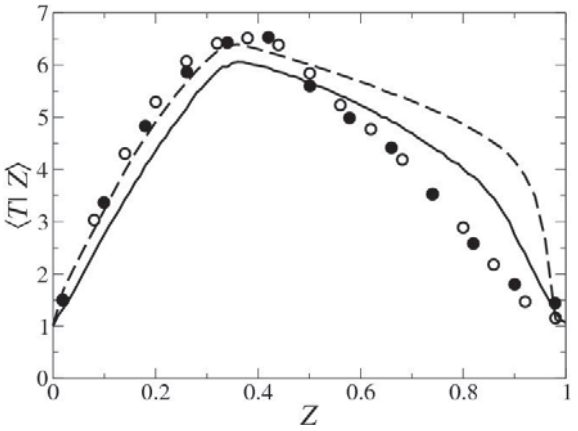

Figure 12: Conditional mean temperature . $x/D = 7.5$::– –: simulation; ○: experiment. $x/D = 15$::——: simulation; ●: experiment.

value of CH_4 in the vicinity of $(0.7 < Z < 0.9)$ as compared to the experimental results together with higher value of temperature in the same region indicates the existence of a fuel rich combustion zone apart from the one at the stoichiometric ratio ($Z = 0.35$). However, no such partially premixed reaction can be observed in the experimental results. This difference in results between temperature and CH_4 is partially due to the absence of sub-grid scale model for reaction/heat-release. The transport equation for both temperature (density) and CH_4 contains the Arrhenius reaction rate equation, which is a highly non-linear term. Such strong non-linearity creates thin flames which cannot be captured on the grid but at the same time they are dynamically important in the sense that they affect the flow field (through temperature rise). Thus this term needs to be evaluated accurately (using a fine grid which captures the flame completely) or they should be modelled in such a way that their effect on the flow field is accounted for correctly. Another reason could be the dissipation associated with the WENO scheme which acts as a sub-grid scale model (Garnier *et al.*, 1999). This allows energy to be transfered to the cut-off wavenumber thereby preventing accumulation of energy at the smallest scales represented on the grid but at the same time have thickened out have the reaction zone. However, such highly non-linear terms are missing in the transport equation for mixture fraction and the inherent dissipation in the WENO scheme is able to correctly account for the sub-grid scale effects. To account for the sub-grid scale effects for the Arrhenius reaction rate an alternative approach would be to include FMDF as a model for the reaction rate term. The FMDF method had been tested in simulations of forced homogeneous turbulence beginning with alternating slabs of fuel and oxidizer as reported previously Chakravorty & Mathew (2007). It was observed that LES with FMDF on a $32 \times 32 \times 32$ grid could track the progress of combustion in step with that of a DNS on a $192 \times 192 \times 192$ grid. In LES with explicit filtering alone, the progress of reaction was initially faster, then slower than the DNS, and also did not achieve the same peak temperature levels. We expect to include a simulation of the jet flame with FMDF and analysis in the presentation.

CONCLUSIONS

LES of reacting turbulent round jet was performed using an explicit filtering method. Results showed that method

accounted for the sub-grid effects of the velocity accurately. However, when this method is used for modeling thin flames, differences arise. The differences were traced to excess combustion in fuel-rich zones. The filtering approach fails to capture the sub-grid scale effects. We expect to overcome this deficiency by adopting a probability density function based closure for the reaction term.

REFERENCES

Akselvoll, K. & Moin, P. 1995 Large eddy simulation of turbulent confined coannular jets and turbulent flow over a backward facing step. *Tech. Rep.* TF-63. Stanford University.

Barlow, R. S. & Frank, J. 2003 www.ca.sandia.gov/TNF.

Boersma, B. J., Brethouwer, G. & Nieuwstadt, F. T. M. 1998 A numerical investigation on the effect of the inflow conditions on the self-similar region of a round jet. *Phys. Fluids.* **10** (4), 899.

Chakravorty, S. & Mathew, J. 2004 A high resolution scheme for low mach number flows. *Int. J. Numer. Meth. Fluids* **46**, 245.

Chakravorty, S. & Mathew, J. 2007 Explicit filtering les for turbulent non-premixed combustion. In *Proceedings of FEDSM2007*. 5th Joint ASME/JSME Fluids Engineering Conference.

Colucci, P. J., Jaberi, F. A., Givi, P. & Pope, S. B. 1998 Filtered density function for large eddy simulation of turbulent reacting flows. *Phys. Fluids* **10** (2), 499.

Garnier, E., Mossi, M., Sagaut, P., Comte, P. & Deville, M. 1999 On the use of shock-capturing schemes for large-eddy simulation. *J. Comput. Phys.* **153**, 273.

Hussein, H. J., Capp, S. P. & George, W. K. 1994 Velocity measurements in a high-reynolds-number, momentum-conserving, axisymmetric, turbulent-jet. *J. Fluid Mech.* **258**, 31.

Jaberi, F. A., Colucci, P. J., James, S., Givi, P. & Pope, S.B. 1999 Filtered mass density function for large-eddy simulation of turbulent reacting flows. *J. Fluid Mech.* **401**, 85.

Jiang, G. S. & Shu, C. W. 1996 Efficient implementation of weighted eno schemes. *J. Comput. Phys.* **126**, 202.

Le, H. & Moin, P. 1994 Direct numerical simulation of turbulent flow over a backward facing step. *Tech. Rep.* TF-58. Stanford University.

Lele, S. K. 1992 Compact finite difference schemes with spectral-like resolution. *J. Comput. Phys.* **103**, 16.

Lowery, P. S. & Reynolds, W. C. 1986 Numerical simulation of a spatially-developing, forced, plane mixing layer. *Tech. Rep.* TF-26. Stanford University.

Majda, M. & Sethian, J. 1985 The derivation and numerical solution of the equations for zero mach number combustion. *Combust. Sci. and Tech* **42**, 185.

Mathew, J., Foysi, H., Sesterhenn, J. & Friedrich, R 2003 An explicit filtering method for large eddy simulation of compressible flows. *Phys. Fluids* **15** (8), 2279.

Panchapakesan, N. R. & Lumley, J. L. 1993 Turbulence measurements in axisymmetric jets of air and helium. Part 1. Air jet. *J. Fluid Mech.* **246**, 197.

Pitsch, H. 2005 Large-eddy simulation of turbulent combustion. *Ann. Rev. Fluid Mech.* **38**, 453.

Pope, S. B. 1982 An improved turbulent mixing model. *Combust. Sci. Technol* **28**, 131.

Stolz, S. & Adams, N. A. 1999 An approximate deconvolution procedure for large-eddy simulation. *Phys. Fluids* **11**, 1699.

Williams, F. A. 1985 *Combustion Theory*, 2nd edn. Reading, MA: Addison-Wesley.

Wygnanski, I. & Fiedler, H. E. 1969 Some measurements in the self-preserving jets. *J. Fluid Mech.* **38**, 577.